OPTICALLY-CONTROLLED SOLID-STATE PLASMA LEAKY-WAVE ANTENNA

Gurvikram Grewal and George W. Hanson
Department of Electrical Engineering and Computer Science
University of Wisconsin-Milwaukee
3200 N. Cramer Street
Milwaukee, Wisconsin 53211

Received 20 May 2003

ABSTRACT: *In this paper, a 2D leaky-wave antenna is designed for millimeter-wave applications in the W band. We consider a method for scanning the antenna beam at a fixed frequency using optical control of the properties of a semiconductor waveguide. The analyses are done at 94 GHz using silicon, although other frequency ranges and materials are possible. Beam scanning is achieved by varying the density of an optically induced plasma, without otherwise modifying the antenna structure or changing the frequency. The steepest-descent approximation is used to calculate the far-field radiation pattern, where we show that the beam can be scanned over an approximately 30° range.* © 2003 Wiley Periodicals, Inc. Microwave Opt Technol Lett 39: 450–453, 2003; Published online in Wiley InterScience (www.interscience.wiley.com). DOI 10.1002/mop.11245

Key words: *leaky-wave; solid-state plasma; optical control*

1. INTRODUCTION

Due to desirable physical characteristics, and spectrum congestion at lower frequencies, millimeter-wave technology has been gaining interest in recent years. The W band of frequencies is of particular importance, as seen by the large number of applications in this area. Devices operating in this band of frequencies generally offer good bandwidth characteristics and compact physical features. Applications of millimeter-wave technology include automotive radars and collision avoidance systems [1], autonomous-landing aircraft systems, satellite communication [2], wireless access systems for subscriber links [3], high-speed wireless LANs, wireless chip-to-chip interconnections for multi-chip modules [4], and missile guidance [5].

Uniform dielectric waveguides are convenient leaky-wave antennas for millimeter-wave applications because they are lightweight, rigid, and easily fabricated from high-purity semiconductors such as silicon and gallium arsenide. Leaky-wave antennas utilizing plasma were among the first leaky-wave antennas studied [6, 7], for application to ionospheric plasma. Later, leaky-wave antenna work centered on layered dielectrics, where material and structural properties could be chosen to result in desirable characteristics [8].

Beyond ordinary dielectric/metallic structures, electronic or other nonmechanical control over radiation characteristics is very desirable. At lower GHz frequencies, ferrites can be used for electronic control over antenna properties [9, 10], although ferrites are generally very lossy in the millimeter-wave range. Solid-state magneto-plasma materials, which are formed by magnetic-field biasing of a semiconductor, are sometimes used in the millimeter-wave regime, although in this case one has control over the imaginary part of the permittivity dyadic, related to conductivity. Another option is a solid-state plasma generated by above-bandgap optical illumination of a semiconductor, leading to optical control over the material's complex permittivity. This scheme has been utilized to optically control various millimeter-wave passive components [11–13]. Solid-state plasmas have also been utilized in antenna applications [14–16], although in these works optically induced gratings were used to produce the leaky-wave radiation.

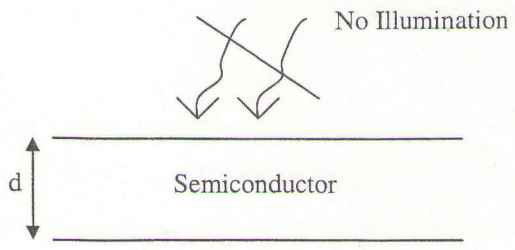

Figure 1 Semiconductor slab without illumination

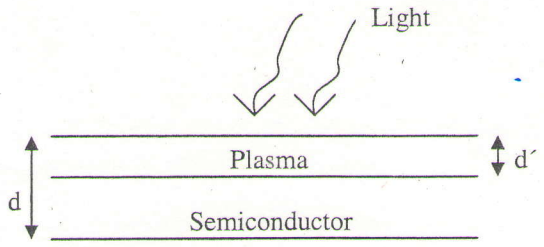

Figure 2 Semiconductor slab with above-bandgap illumination

In this paper, we consider a 94-GHz optically controlled leaky-wave antenna based on a simple silicon-waveguide structure. Steering of the main beam has been achieved by optically varying the plasma density, which affects the leaky-wave propagation constant of the background dielectric waveguide, thereby controlling the radiation pattern.

2. FORMULATION

Consider a semiconductor slab in the absence of any illumination, as shown in Figure 1, and the case where the semiconductor slab is illuminated by above-bandgap radiation, as shown in Figure 2. When the semiconductor waveguide is illuminated with above-bandgap radiation, a plasma layer is created within the region d', the refractive index of which differs greatly from that of the background semiconductor. The real and the imaginary parts of the refractive index $n = \eta - j\kappa$ are given by [11]:

$$\eta^+,\ \kappa^- = \left\{ \pm \frac{1}{2}\left(\varepsilon_L - \frac{\omega_p^2}{\omega^2+\nu^2}\right) + \frac{1}{2}\left\{\left(\varepsilon_L - \frac{\omega_p^2}{\omega^2+\nu^2}\right)^2 + \left(\frac{\omega_p^2}{\omega^2+\nu^2}\frac{\nu}{\omega}\right)^2\right\}^{1/2}\right\}^{1/2}, \quad (1)$$

where η and κ are obtained by selecting the + or − sign in the leading term in Eq. (1), respectively. In Eq. (1), ε_L is the dielectric constant of silicon, ν is the collision frequency in the plasma, ω is the operating frequency, and ω_p is the plasma frequency, given by

$$\omega_p = \sqrt{\frac{Ne^2}{\varepsilon_0 m^*}}, \quad (2)$$

where N is the density of plasma per cm^3, e is the electronic charge, and m^* is the effective mass of the charge carrier. The dielectric constant of the plasma is $n^2 = \varepsilon_{plasma}$.

The real and imaginary parts of the plasma as a function of plasma density N are shown in Figure 3.

As can be seen from Figure 3, when N is approximately equal to 10^{15}/cm^3, the real part of the refractive index begins to deviate

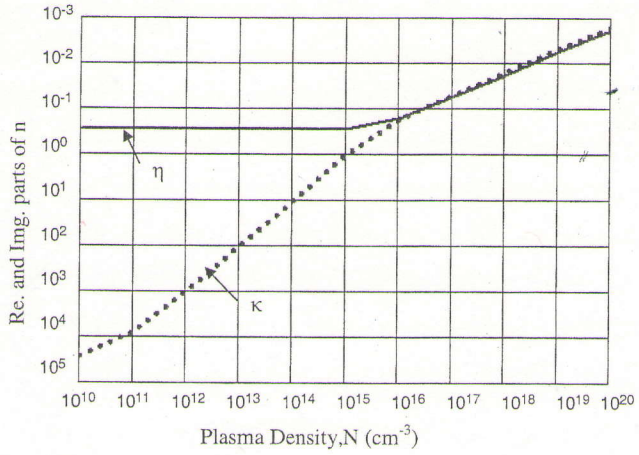

Figure 3 Variation of complex refractive index of plasma as a function of plasma density

from its low-density value, and at $10^{16}/cm^3$ the real and the imaginary parts become approximately equal. Above this density, the plasma begins to act like a metal. The plasma density and thickness are controlled by the intensity of the optical illumination.

From the above discussion, it is obvious that a plasma layer can be induced in a semiconductor, and the properties of the plasma controlled externally. Based on this phenomenon, Figure 4 shows a 2D leaky-wave antenna consisting of a line source, a silicon layer, and optical illumination.

Varying the plasma density (which is, in turn, dependent upon the intensity of the laser illuminating the silicon slab) changes the permittivity of the plasma. The antenna's properties are varied from the underside, rather than from the primary radiation side (the air region above the structure), which is an advantage, since any mechanical structure to produce the incident illumination will not interfere with radiation. A drawback, though, is that at low plasma densities the antenna will radiate into both upper and lower half-spaces, although for sufficiently high densities the plasma region is essentially a metal, and radiation occurs only into the desired upper half-space.

For numerical computations, the thickness of the plasma layer was chosen to be 50 μm, which is a reasonably obtainable value. The thickness of the silicon was taken to be $10\lambda_{si}$, where λ_{si} is the wavelength in silicon at 94 GHz. An increase in waveguide thickness beyond this value would result in side-lobe radiation. The line source is positioned at the top of the silicon layer, at the air/silicon interface.

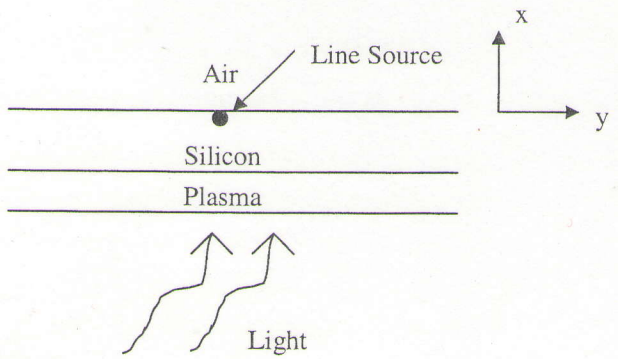

Figure 4 Leaky-wave antenna geometry

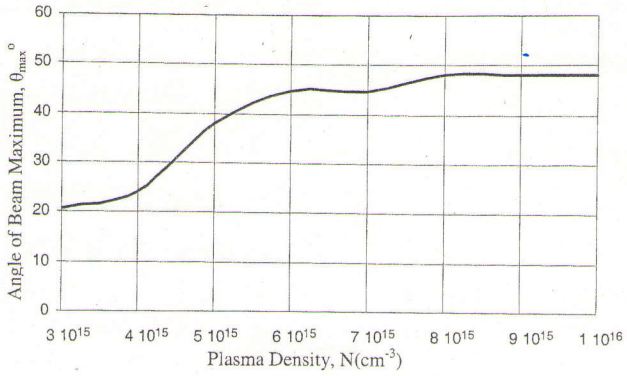

Figure 5 Variation of angle of beam maximum vs. plasma density

The electric field in the air region, due to a TE line source, is given by

$$\vec{J}(x, y) = \hat{z} I_0 \delta(x)\delta(y), \tag{3}$$

and in the silicon region is

$$\vec{E}(x, y) = \hat{z} I^e(x, y), \tag{4}$$

when

$$I^e(x, y) = I_0 \int_{-\infty}^{\infty} G(k_y) e^{-px} e^{jk_y y} dk_y. \tag{5}$$

In Eq. (5), $p = \sqrt{k_y^2 - k_0^2}$, where k_0 is the free-space wave number. The coefficient $G(k_y)$ has a complicated form, and is given in [17]. The integral in Eq. (5) is solved using the steepest-descent approximation, leading to

$$I^e = I_0 \frac{\sqrt{2\pi}}{\sqrt{kr}} e^{-jkr} e^{j(\pi/4)} F(\phi_s), \tag{6}$$

where r is the radial distance from the antenna, $F(\phi_s) = G(\phi_s)k_0 \cos \phi_s$, and ϕ_s is the saddle point, $\phi_s = \theta$, with θ the angle measured from the vertical (x) axis.

Figure 5 shows the beam scan as the plasma density varies. It can be seen that the major scan occurs between $10^{15}/cm^3$ and $10^{16}/cm^3$. The beam angle, below $10^{15}/cm^3$ and above $10^{16}/cm^3$, remains approximately constant. Therefore, we can scan the beam over a 30° range with only a small change in the density of the plasma.

TABLE 1 Values of θ_{bp} with Respect to Various Plasma Densities and Corresponding Q Values

Density (/cm^3)	θ^o_{bp}	Q (1)	Q (3)	Q (7)	Q (10)
$1/10^{14}$	20.70	0.563	3.991	26.465	71.984
$1/10^{15}$	20.10	0.440	3.328	25.119	75.283
$4/10^{15}$	26.50	0.171	1.431	13.176	45.830
$5/10^{15}$	35.30	0.203	1.561	12.175	37.393
$6/10^{15}$	41.00	0.454	3.256	22.063	60.989
$1/10^{16}$	48.50	0.395	2.513	13.412	30.999

TABLE 2 Comparison Between θ_{bp}, the Leaky-Wave Predicted Beam Angle, and the Actual (Simulated) Beam Angle, θ_{max}

Density (/cm^3)	θ^o_{bp}	θ^o_{max}
$1/10^{14}$	20.70	20.62
$1/10^{15}$	20.05	20.62
$4/10^{15}$	26.49	24.06
$5/10^{15}$	35.32	37.82
$6/10^{15}$	41.02	44.69
$1/10^{16}$	48.52	48.12

3. LEAKY-WAVE ANALYSIS

As is well known, leaky-wave antennas have radiation properties that can be explained in terms of the background waveguide's leaky waves. In converting Eq. (5) to the steepest-descent plane, and moving the integration contour to the steepest-descent contour, proper and improper waveguide poles may be captured. These field (residue) constituents do not directly contribute to the far field in a steepest-descent approximation (except along the interface), although leaky waves may dominate the near field. In this case, a convenient alternative method to determine the far field is via the Kirchhof–Huygens integration of the near field [7], from which one sees that if the near field is dominated by a leaky wave, the corresponding far-field behavior is explained by the leaky wave.

Let θ_{max} be the angle of maximum radiation, as shown in Figure 5. In [7] it is shown that

$$\theta_{bp} = \cos^{-1}\left(\sqrt{\cosh^2\phi_r - \sin^2\phi_i}\right) \tag{8}$$

is the angle of the main beam as predicted by the leaky wave, where $\phi_p = \phi_r + j\phi_i$ is the steepest-descent variable evaluated at the leaky-wave pole location.

In Table 1 we provide the values of θ_{bp} for different plasma densities. The value Q in the table corresponds to the ratio of the pole contribution (residue contribution) to the excitation amplitude of the space wave of Eq. (6), which must be much greater than unity for the leaky wave to dominate the far field [7]. The value within the parentheses is the distance from the line source (y) at $x = 0$ along the surface of the waveguide, in millimeters. Since the leaky wave clearly dominates, we expect that the radiation properties of the antenna can be adequately described by the leaky-wave theory.

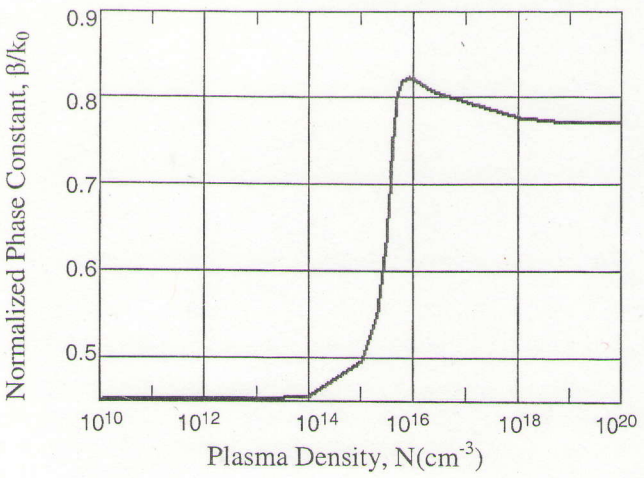

Figure 6 Normalized phase constant with respect to plasma density

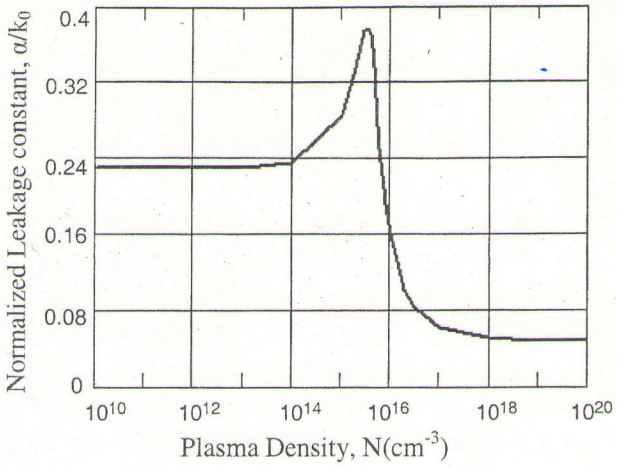

Figure 7 Normalized leakage constant vs. plasma density

To verify this statement, Table 2 provides a comparison between θ_{bp} and θ_{max} for different plasma densities, where θ_{max} is the angle of the beam maximum computed from the steepest-descent result [Eq. (6)]. It can be seen that the leaky mode clearly controls the far-field behavior, since θ_{bp} is approximately equal to θ_{max} in all cases.

For wave propagation of the form $e^{-j(\beta - j\alpha)z}$, the variation of the normalized phase constant and leakage constant of the silicon/plasma waveguide with plasma density is shown in Figures 6 and 7, respectively [17]. In Figure 6, the most significant variation of the phase constant occurs between the densities 10^{15}/cm^3 and 10^{16}/cm^3. It can be seen that as the density increases from 10^{15}/cm^3 to 10^{16}/cm^3, the phase constant changes rapidly, which, in turn, controls the beam-scan angle, as shown in Table 2.

In Figure 7, we show the variation of the leakage constant versus plasma density. A large value of the leakage constant implies a large leakage rate, thus producing a short effective aperture, so that the radiated beam has large beamwidth. Conversely, a low leakage-constant value results in a narrow beam, provided that the physical aperture is sufficiently long. As can be seen from Figure 7, the beam narrows at higher plasma densities.

4. CONCLUSION

This paper describes a method for scanning the main beam of a simple solid-state plasma leaky-wave antenna at 94 GHz by optically controlling the density of plasma in the semiconductor slab. The main beam can be scanned by approximately 30° at a fixed frequency. Simulation results for the beam scan are provided, as are results that verify the leaky-wave nature of the antenna.

REFERENCES

1. I. Gresham, N. Jain, T. Budka, A. Alexanian, N. Kinayman, B. Ziegner, S. Brown, and P. Staecker, A 76–77 GHz pulsed-doppler radar module for autonomous cruise control applications, IEEE Microwave Symp Dig MTT-S 3 (2000), 1551–1554.
2. P. Staecker, Device technology and integration techniques for commercial MM-wave systems, IEEE Topical Symp on Millimeter Waves, 1997, pp. 51–54.
3. H. Izadpanah, A millimeter-wave broadband wireless access technology demonstrator for the next-generation internet network reach extension, IEEE Commun Mag (2001), 140–145.
4. M.K. Iyer, R.D. Seager, and J.C. Vardaxoglou, Wireless chip to chip interconnections for multichip modules using leaky wave antennas, Electron Lett 29 (1993), 2030–2031.
5. W.R. Deal, T. Jung, C. Ming, and T. Itoh, All-optically controlled

beam steering array for antenna remoting applications, IEEE MTT-S Dig (1998), 1383–1386.
6. T. Tamir and A.A. Oliner, The influence of complex waves on the radiation field of a slot-excited plasma layer, IRE Trans Antennas Propagat 10 (1962), 55–65.
7. T. Tamir and A.A. Oliner, Guided complex waves part-1: Fields at an interface, and part-2: Relation to radiation patterns, Proc IEE 110 (1963), 310–334.
8. D.R. Jackson, A.A. Oliner, and A. Ip, Leaky-wave propagation and radiation for a narrow-beam multiple-layer dielectric structure, IEEE Trans Antennas Propagat 45 (1997), 1294–1301.
9. P. Bacarelli, C. Di Nallo, F. Frezza, A. Galli, and P. Lampariello, The role of complex waves of proper type in radiative effects of nonreciprocal structures, IEEE MTT-S Dig (1997), 491–494.
10. I.Y. Hsia and N.G. Alexopoulos, Radiation characteristics of hertzian dipole antennas in a nonreciprocal superstate-substrate structure, IEEE Trans Antennas Propagat 40 (1992), 782–790.
11. C.H. Lee, P.S. Mak, and A.P. De Fonzo, Optical control of millimeter-wave propagation in dielectric waveguides, IEEE J Quantum Electron QE-16 (1980), 277–288.
12. A.M. Vaucher, C.D. Striffler, and C.H. Lee, Theory of optically controlled millimeter wave phase shifters, IEEE Trans Micro Theory Tech MTT-31 (1983), 209–216.
13. S.K. Dana, H. Shimusaki, and M. Tsutsumi, Efficient optical control of millimeter waves in a slot line on semiconductor plasma substrate, IEEE Trans Micro Theory Tech 50 (2002), 207–210.
14. M. Matsumoto, M. Tsutsumi, and N. Kumagai, Radiation of millimeter waves from a leaky dielectric waveguide with a light-induced grating layer, IEEE Trans Micro Theory Tech 45 (1987), 1033–1041.
15. V.A. Mansson, L.S. Sadovnik, V.A. Yepishin, and D. Marker, An optically controlled mmw beam-steering antenna based on a novel architecture, IEEE Trans Micro Theory Tech 45 (1997), 1497–1500.
16. A. Alphones and M. Tsutsumi, Leaky wave radiation from a periodically photoexcited semiconductor slab waveguide, IEEE Trans Micro Theory Tech 43 (1995), 2435–2441.
17. G.S. Grewal, Solid state plasma leaky wave antenna, M.S. thesis, University of Wisconsin–Milwaukee, 2003.

A NOVEL FRACTAL DEFECTED GROUND STRUCTURE AND ITS APPLICATION TO THE LOW-PASS FILTER

Hai W. Liu,[1,2] Zheng F. Li,[1] and Xiao W. Sun[2]
[1] Department of Electronic Engineering
Shanghai Jiaotong University
Shanghai 200030, P. R. China
[2] Shanghai Institute of Microsystem and Information Technology
Chinese Academy of Sciences
Shanghai 200050, P. R. China

Received 18 May 2003

ABSTRACT: *A novel fractal defected ground structure (DGS) for the microstrip line is proposed. The DGS unit lattice is realized by replacing the etched rectangular holes in ground plane with a Sierpinski carpet. The proposed fractal DGS can provide better bandgap, slow-wave characteristics, and selectivity at cutoff than the conventional dumbbell-shaped DGS. Furthermore, the fractal DGS is applied effectively to design a low-pass filter (LPF). A comparison between simulation and measurement confirms the validity of the LPF configuration and design procedure. A simple structure and high-power handling capability are obtained from the proposed LPF.* © 2003 Wiley Periodicals, Inc.
Microwave Opt Technol Lett 39: 453–456, 2003; Published online in Wiley InterScience (www.interscience.wiley.com). DOI 10.1002/mop.11246

Key words: *defected ground structure; bandgap; fractal; low-pass filter; slow-wave; selectivity; Sierpinski carpet*

1. INTRODUCTION

Defected ground structure (DGS) for the microstrip line, which has etched defects in the backside metallic ground plane, has recently become popular for the design of microwave circuits [1] because of its excellent bandgap characteristics and ease of fabrication with photolithographic MIC, MMIC, and MEMS processes. Compared to photonic bandgap (PBG) [2], DGS has a simple structure and potentially great applicability to the design of microwave circuits such as filters, amplifiers, and oscillators [3–6]. The electromagnetic waves in DGS materials provide bandgap characteristics, hence making a slow-wave structure. In slow-wave structures, the effective wavelength increases without any dimensional changes, thus a compact design is obtained.

In previously reported DGS, the DGS lattice had a simple geometrical shape, for example, rectangular. In this paper, a novel fractal DGS lattice, which is composed of a Sierpinski carpet, is proposed. The fractal DGS section can be performed as a series LC resonator by using a simple circuit-analysis method. Also, the behavior of fractal DGS-engineered material can be controlled by a lattice parameter, such as the filling factor. Simulations show its bandgap and slow-wave characteristics are better than those of the conventional dumbbell-shaped DGS.

Moreover, the fractal DGS is applied effectively to the design of a low-pass filter (LPF). This LPF is designed and fabricated with one DGS pattern on the ground plane and a 50Ω microstrip line with two cross-junction open stubs on the top metal plane. A comparison between simulation and measurement confirms the validity of the proposed fractal DGS and the LPF's configuration and design procedure. Simple structure and high power handling capability are obtained from the proposed LPF.

2. FRACTAL DGS PATTERN AND ITS BANDGAP CHARACTERISTICS

Figure 1 shows the schematics of the proposed fractal DGS and a conventional dumbbell-shaped DGS, occupying the same surface area. The DGS is etched on the metallic ground plane. The fractal DGS lattice shown in Figure 1 possesses the some self-similarity as a Sierpinski carpet, and shows some fractal characteristics [2]. Generally speaking, the important design parameters of DGS are the etched lattice dimension $a \times a$ and the gap distance g. Moreover, the proposed fractal DGS provides another important design parameter—filling factor a_1/a_2, where the relationship $2a_1 + a_2 = a$ is selected for simplicity. The substrate for simulation and measurement was an RT/Duroid 5880 with 0.762-mm thickness and a dielectric constant ε_r of 2.22. The line width w is chosen for the characteristic impedance of the 50Ω microstrip line. The DGSs are simulated via the method of moments (MoM) using Ansoft Ensemble 8.0 SV.

Figure 2 shows the simulation of the transmission characteristics of three different filling factors $a_1/a_2 = 1/3$ ($a_1 = 0.9$ mm), $a_1/a_2 = 1$ ($a_1 = 1.5$ mm), and $a_1/a_2 = 2/1$ ($a_1 = 1.8$ mm) for the fractal DGS, compared with a dumbbell-shaped DGS ($a = 4.5$ mm). The simulation shows the attenuation poles of the fractal DGS shift lower than that of the dumbbell-shaped DGS in the same occupied surface. In addition, the fractal DGS provide sharper cutoff performances.

Figure 3 shows the equivalent circuit of the proposed fractal DGS. The bandgap characteristics can be explained by a parallel LC resonator (L_r and C_r). The radiating effects are taken into account and represented by R_r. The equivalent circuit parameters can be derived from the S parameters based on the electromagne-